International Journal of Fracture and Damage Mechanics
Vol. 1: Issue 2
www.journalspub.com

Stress and Fatigue Damage Computation of a Nose Landing Gear

K. L. Singh[1] and Abdul Waheed. A.*[2]
[1]STTD, CSIR-National Aerospace Laboratories, Kodihalli, Bangalore, India
[2]AE, M V J College of Engineering, Channasandra, Bangalore, India

Abstract

In this paper, the modeling of a Nose Landing Gear (NLG) is done using 1D beam elements and 3D tetrahedral elements. The h-type convergence simulation has carried out in three sizes of elements as 2.5, 5 and 10 mm for beam elements. In the 1D beam element model, the modeling of bearing is done with one and two Multi Point Constraint (MPC) elements. The stresses from the 1D model with one and two MPCs, and 3D element model results were compared. Experimental strain values are compared with the 1D and 3D NLG models. The Fatigue Damage computation is presented using Stress-Life (S-N) approach the stress combination used are Maximum principal, von-Mises, and Critical plane. Simulation has been done with mean and without mean stress correction. The fatigue damage/ life benchmark problem of a plate with a hole is simulated for three configurations of full, half and quarter models. The stresses and damage results for the three configurations are the same. The stress results of NLG with the fatigue material properties and lateral drift loading spectrum are analyzed using multi-axial fatigue damage algorithms.

Keywords: nose landing gear, finite element analysis, experimental, multi-axial fatigue, mean stress correction

**Corresponding Author*
Email ID: krishna_lok@yahoo.com

INTRODUCTION

During World War I, the landing gear configuration had more or less settled down to the tail wheel type. Until World War II most aircraft had fixed type of landing gears, often with exotic-looking spats to reduce drag. Landing gears are generally categorized by the number of wheels and their pattern. In this article discussed about the tri-cycle type. In this, the nose wheel has twin number of wheels. The entire aircraft is supported by the Landing gear during landing and ground operation, as they are attached to the primary structural members of the aircraft. [1] The nose gear carries about 10–20 percent and the main gear carries 80–90 percent of the total take-off load of an aircraft. Design and stress analysis of nose landing gear barrel of typical naval trainer aircraft utilizing FEA is presented in the reference. [2] The computation of loads is from the Federal Aviation Administration formulas. [3, 4]

Elastic finite element analysis typically provides estimates of the working stresses. [5] In this article, some of the stress-based models are used as the landing gears do operate near, above or below the fatigue threshold. [6] Prescience life of MLG under multiaxial loading with lateral drift landing cases is employed for the determination of equivalent stress and Palmgren Miner's theory used for calculating aggregate damage. [7] A new fatigue failure criterion so called critical plane orientation is correlated with multiaxial high-cycle

fatigue and the criteria is analyzed and compared with experimental data for different brittle metals. [8] Different methods of Multiaxial fatigue criteria is being employed to predict the overall tendency life of the component using the PragTic freeware fatigue solver. [9] Multiaxial fatigue assessments was carried out with the help of an appropriate rule that reduces the complex multiaxial loading to and equivalent uniaxial loading. [10]

In this article, stress analysis numerically computed strain values are compared with the experimental strain gauge results for NLG in the first part. In the second part of the NLG, it is subjected to multiaxial loading conditions and computed the damage and its corresponding life using different equivalent stress-based models in MSC Fatigue.

DEVELOPMENT OF FINITE ELEMENT MODEL

Landing Gear Geometry

The nomenclature of various components of a typical Nose Landing Gear (NLG) model is set out in Figure 1. Figure 2 depicts the free edges of a typical NLG this confirms that there are no cracks or free edges in between the components. This figure shows the complexity of the problem with 125, 67 and 37 numbers of full, half and quarter circular edges respectively. The complex difficulty lies in meshing the geometry manually; hence auto-mesh is preferred. The free edges check is an important step to start with the meshing. The NLG structure model's meshing detail shall be examined in the following sections.

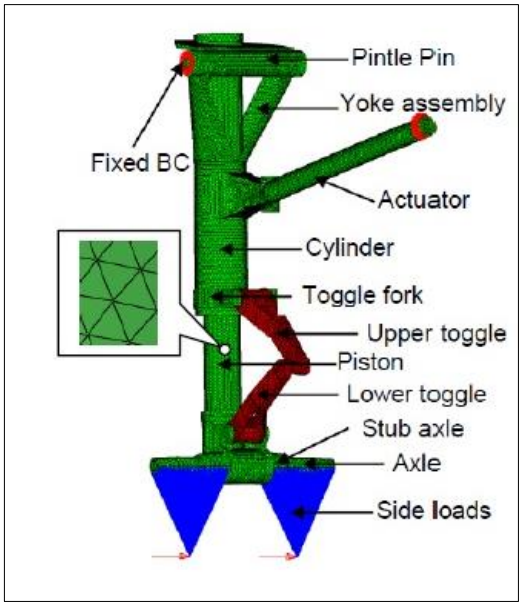

Fig. 1: *Development of Finite Element Model- Landing Gear Geometry.*

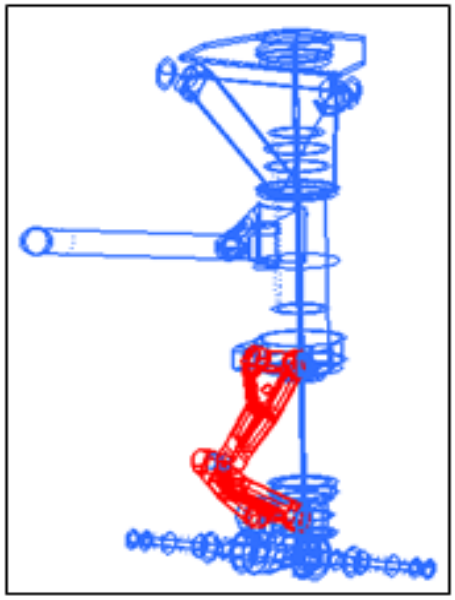

Fig. 2: *Free Edges Model of a NLG.*

In this article, the shock absorber (piston and cylinder) position is always maintained at 100 mm. There is no change in the position of the piston and cylinder. NLG line model analysis is also carried out using 3D Beam elements in ABAQUS 6.12 [11] with two different connectivity of MPC beam between piston and cylinder at distance 48.3 from the top of the piston for one case and for the other 2 MPC are used at the 30.0 mm distance from 29 mm from piston and the results are compared with NLG 3D model as the connectivity between piston and cylinder is at the

coordinate (38.706, 7.878, –1151.570) and (38.706, 7.878, –1181.570) this is at distance of 30.0 mm.

Material Properties

The NLG is made up of two materials, viz., MANTEN-MSN steel and Aluminum-2024-HV-T3. These two materials are mechanical and fatigue properties are listed in Table 1. The landing gear chosen for this study is mainly composed of steel except the toggle links are of Aluminium material. [12]

Table 1: *Mechanical and Fatigue Properties.*

Mechanical / Fatigue Properties	Aluminium-2024-HV-T3	MAANTEN-MSN
Ultimate Tensile strength (MPa)	490	600
Yield Strength (MPa)	275	250
Young's Modulus (GPa)	72	210
Poisson's ratio	0.334	0.3
Density (Kg/m^3)	2830	7890
Stress Range Intercept (MPa)	2038	8984
First Fatigue strength exponent	–0.1002	–0.2
Fatigue transition Point (cycles)	1E06	2E08
Second Fatigue strength exponent	–0.1002	0
Standard Error of Log (N)	0	0.137
Stress Ratio (R)	–1	1

Finite Element Models

One Dimensional Beam Model

Nose Landing Gear is modeled by specifying various cross sections like rectangular, I and pipe sections as per the requirement. The details of various components and their section profiles are listed in Table 2. Figure 3 is the superimposed model of beam elements with its profile. The 3D beam elements are represented as B31 in ABAQUS software. [11] Figure 4 depicts the boundary conditions and loading details for the NLG beam model.

Table 2: *Beam Pipe Section Profiles and their Dimensions.*

S. No.	Component	Beam cross-section profiles	
		Radius, mm	Thickness, mm
1	Cylinder	57.5	9.5
2	Piston	39.55	5.0
3	Stub-axle	49	9.5
4	Actuator	22.15	5.6
5	Pintel Pin	25.5	7.0
6	Yoke	30.0	5.0
7	Axle	25.5	7.0

On the Toggle fork, stub fork and top support modeled with rectangular sections. The dimensions of Toggle and stub fork are having broad as 51 mm and height as 17.95 mm. The top supports dimensions, broad as 278 mm and height of 10.0 mm. The toggle links modeled with I-section with the dimensions of the top and bottom flanges breadth as 50 mm and height of 7.0 mm, and web thickness is 3.0 mm. The dimensions of centroid and total height of the I-section are 17.0 mm and 34.0 mm respectively.

The variation in the toggle link cross-section could not be simulated as this is limitation of beam/ stick elements (1D) model.

These are useful especially in the case where the exact cross-section details are not available for modelling. Generic section profiles are assigned to stick/ beam

model render graphical display as showed in Figure 3. It looks like that of the mesh of three-dimensional (3D) elements model.

The NLG model is auto meshed with tetrahedral (C3D4, inset zoomed view of the mesh) elements as shown in Figure 1.

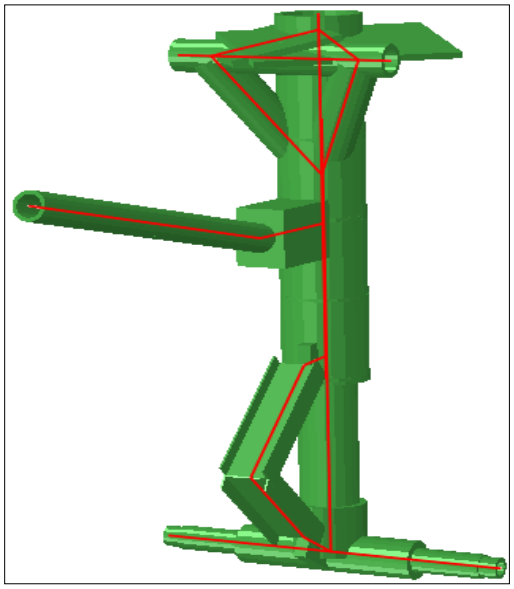

Fig. 3: *Line Model Superimposed With Beam Profile.*

Auto mesh is preferred as the interaction of components like the sub axle and the piston region joining, toggle links joining, and the top toggle link to the piston connections are complex manual meshing is most difficult.

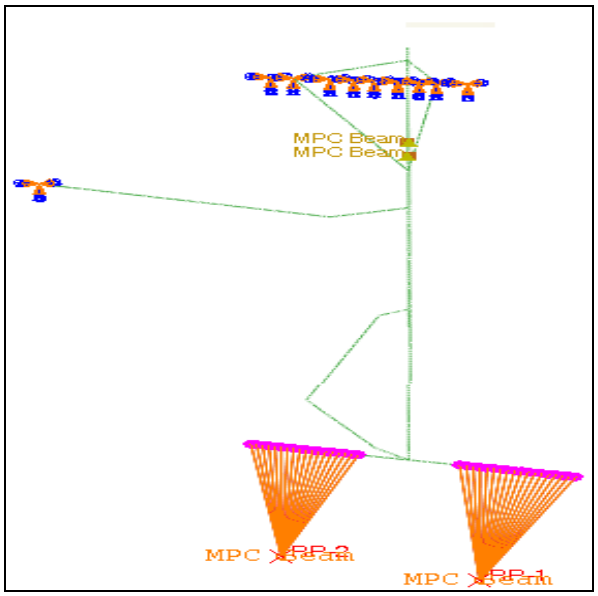

Fig. 4: *Boundary Condition and Loading.*

Bearing Modeling, in the 1-D beam model modeling of bearing is accomplished with MPC. The height of bearing is 30 mm is shown in Figure 5, CAD cross sectional view. The cross-sectional view of the 3D tetra mesh is shown Figure 6 indicating the bearing in this case there is no need of MPC element.

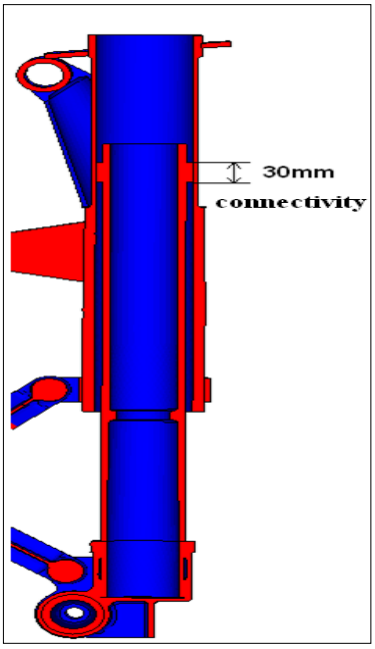

Fig. 5: *Full Length Cross Sectional View.*

Fig. 6: *Partial Length Cross Sectional View.*

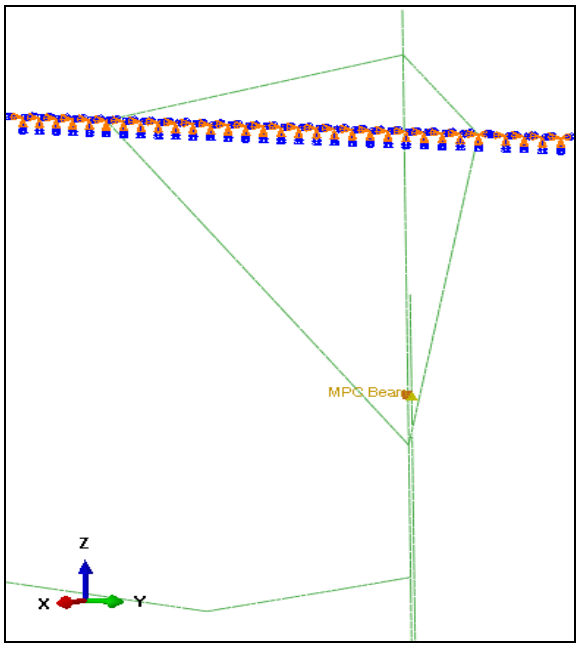

Fig. 7: *NLG Model with One MPC Connectivity.*

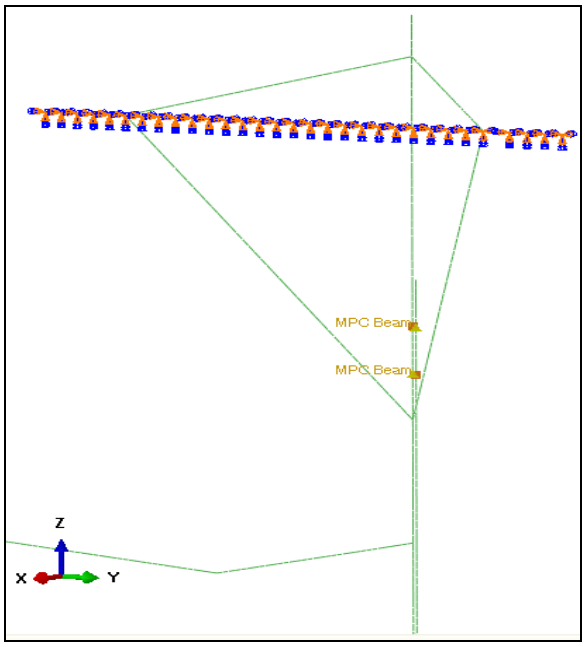

Fig.8: *NLG Model with Two MPC Connectivity.*

Figures 7 and 8 are the one-dimensional line models with one and two MPCs for the bearing. It is understood that the one MPC as showed in Figure 7 situated at the lowest point of contact and a myriad (many) of MPCs placed above it yield the same result. There is not any difference in the output of stress.

Three Dimensional Tetrahedral Model

Geometric models are generated in Catia V5 is imported to Hypermesh [13] where the CAD model as showed in Figure 2 is cleaned up and meshed with Tetrahedral [14] Elements. Finite Element 3D model was solved using MSC NASTRAN 2013.1 CAE Software [15] for stress and displacement as per Load data provided by Landing gear design group.

From the landing gear strength calculations, we obtained the stress spectrum which is necessary for Fatigue analysis carried out using MSC Fatigue Durability module in MSC PATRAN 2012. [15] The output from Fatigue analysis is either life in cycles or a Safety Factor depending on the type of analysis was conducted.

Loading and BC

The boundary conditions applied are the actuator and upper yoke assembly are fixed to the fuselage as showed in Figure 4. The loads applied are uniform and equally distributed on either side of axle nodes.

Even line edge loads are applied and numerical analysis renders the same results as that of the uniform load. In order to check the accuracy of the results, the numerical simulation was done with linear beam element (823 nodes) performing h-type of convergence study. The h-type of convergence the stress variation was within less than 1% deviation.

Since, they are different loading conditions among them are spin up, spring back, maximum vertical and lateral drift landing cases as described in FAR-25. [16] In this paper, spin up and lateral drift cases have been taken on line and solid model of NLG for checking the accuracy of the results of the numerical simulation was done.

The Landing gear design group loads are applied on the axle part X (Drag) and Z (Vertical) direction for Spin-up Case and X (Drag), Y (Side) and Z (Vertical) direction for Lateral Drift Case i.e., X and Z directions are applied on the axle part and side loads is applied at tires as per FAR-25 [16] using RBE3 (Rigid Body Element). The landing load cases given by Landing gear design group are presented in Table 3. Figure 1 shows the Finite Element model, Boundary Conditions (BC) and loading for NLG. The Load applied for different cases in showed in Table 3.

Mesh convergences studies of spin up case with 1MPC beam are carried out and the results are tabulated in Table 4.

***Table 3**: Landing Load Cases for Nose Gear.*

S. No.	Loading cases	Drag load	Side load	Vertical load
1	Spin-up	5943.95	0	7429.93
2	Lateral drift	5611	3511.98	14038.11

***Table 4:** Mesh Convergences Studies for Spin-up Case for 1MPC Connectivity.*

Element size	Deflection (mm)	Stress (MPa)	Nodes	Elements
10	2.520	185.7	409	411
5	2.567	192.2	823	825
2.5	2.590	192.7	1651	1651

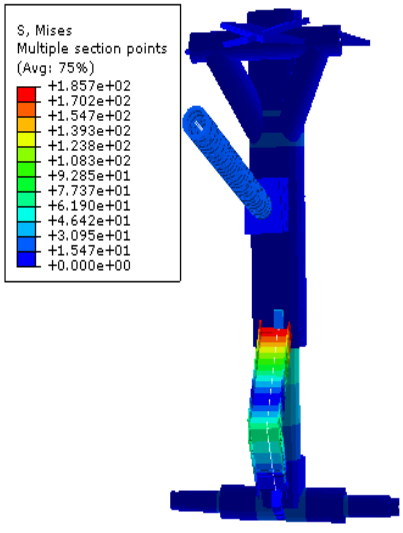

***Fig. 9a:** Line Model with Element Size 10*

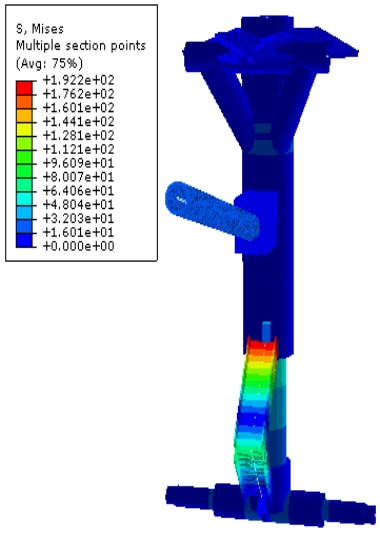

***Fig. 9b:** Line Model with Element Size 5*

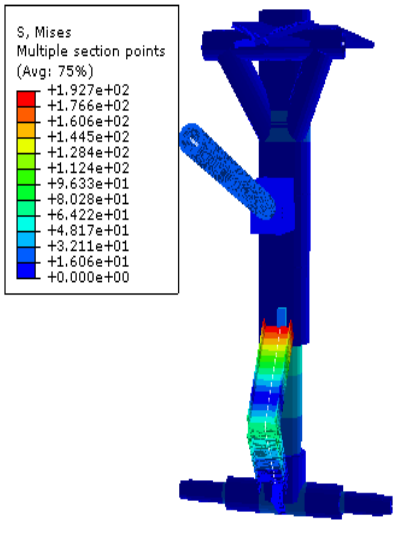

***Fig. 9c:** Line Model with Element Size 2.5*

***Fig. 9:** Convergence Study Mesh Size and Results.*

For h-type Convergence is completed by reducing the element size from 10, 5 and 2.5 mm in steps of h/2.

Element type chosen in ABAQUS software is B31-beam. A mesh convergence is carried out for different element size on 1MPC Line model for Spin-up case as showed in Figure 9a, 9b and 9c with element (B31-beam) size of 10, 5 and 2.5 respectively and the results are tabulated in Table 4. Element size 10 mm the maximum stress magnitude is 185.7 and for 5 mm it is 192.2 and for 2.5 mm, it is 192.7.

The percentage variation decreases from 3.38 to 0.26. It is seen that the convergence is achieved as we have finer mesh. Similarly, the stress plot for line model of NLG for lateral drift and spin up is shown in Figure 10 and 11 respectively.

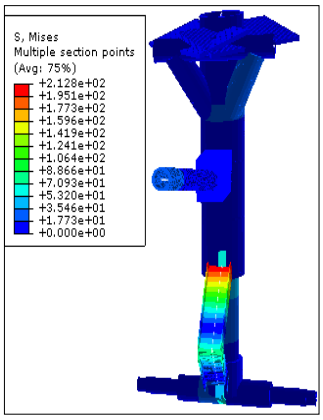

Fig. 10: *Stress plot of Line model NLG-Lateral Drift.*

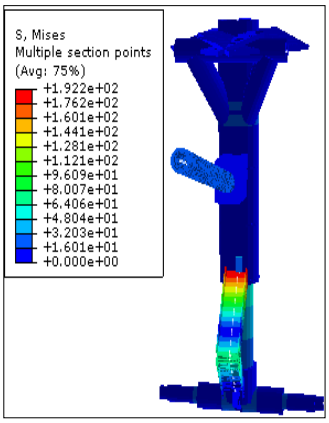

Fig.11: *Stress Plot of Line model- Spin-up.*

It is seen that for tetrahedral configuration with uniform loading on either side of the axle, hence, the total number of elements of 3D NLG is 1 63 364 (Nodes 47 995) which consists of 1 43 985 DOF's mesh render optimal results as showed in Figure 11. Stress plot results obtained for lateral drift and spin up is also shown in Figures 12 and 13 respectively. By applying the appropriate loading and retaining boundary constraints the results for different load cases is also tabulated in Table 5.

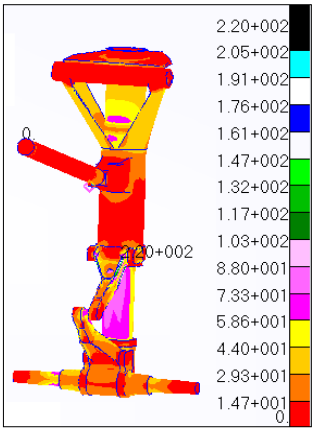

Fig. 12: *Stress Plot of 3D NLG Lateral Drift.*

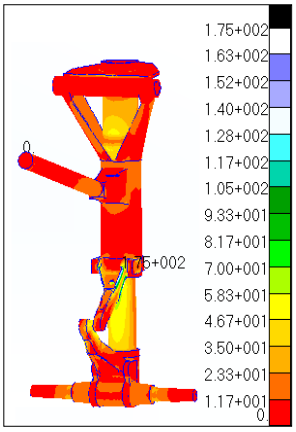

Fig. 13: *Stress Plot of 3D NLG Spin-up.*

Table 5: *MPC Models of Beam and Solid Models Comparison of Displacement and Stresses.*

S. No.	Load cases	1MPC Beam		2MPC Beam		Solid Model	
		Displacement (mm)	Stress (MPa)	Displacement (mm)	Stress (MPa)	Displacement (mm)	Stress (MPa)
1	Steering	4.149	60.34	4.139	60.34	2.65	78.7
2	Max. Vertical	0.8623	59.17	0.8617	59.17	1.21	72.4
3	Spin-up	2.569	192.2	2.567	192.2	2.97	175
4	Spring Back	2.641	190.9	2.639	190.9	2.97	175
5	Lateral Drift	5.497	211.8	5.489	211.8	5.863	220

Experiment Details

In experimental configure, Landing gear was mounted vertically in the test rig in the same attitude as in aircraft. Compression of shock absorber maintained was 100 mm for NLG. Applying loads of different directions, a specially designed loading assembly was used which was fitted into the axle. This assembly had provisions and locations for the application of vertical, side and drag loads.

Loads were monitored using load cells & measurement of deflection; specially designed graph papers were used. Strains were measured for NLG by strain gauges located near axle, stub axle, yoke bottom, top support and cylinder; these are in turn connected to a data logger. Micro strain data obtainable from Strain gauges are compared with strains from FE analysis numbers highlighted in Figure 14 indicates strain gauge locations and Figure 15 shows the strain plot of NLG.

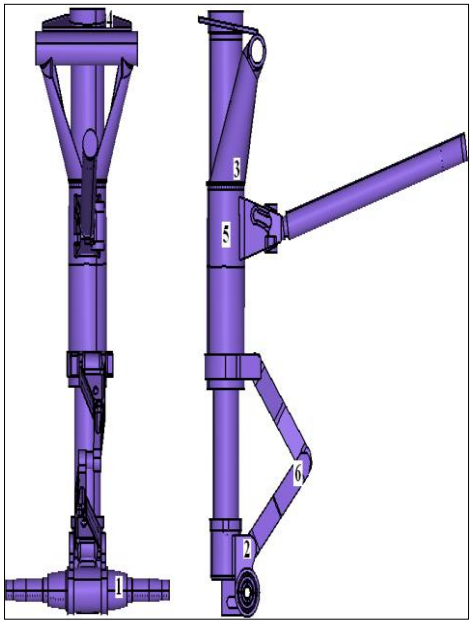

Fig. 14: *Strain Gauge Locations-NLG.*

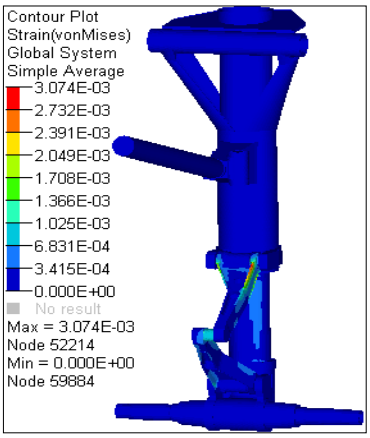

(a) NLG model depicts the strain distribution

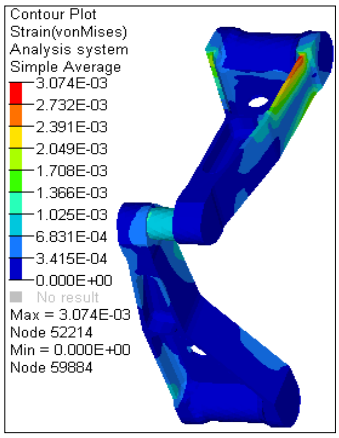

(b) Toggle links of NLG model

Fig. 15: *Strain Plots of a Nose Landing Gear.*

The maximum stress and strain in the linear static analysis occur at the same location as seen in Figures 12, 13 (stress plot) and 15 (strain plots). A typical way of looking at the maximum strain values is given in Figures 16 and 17 only for the axle and toggle components respectively and comparison of the experimental results with the FE strain results is tabulated in Table 6. The stress behavior and the displacement of a nose gear of an aircraft during landing using structural finite element analysis determined.

Table 6: *Comparison of FEA and Experimental Data for Lateral Drift Case.*

S. No.	Locations	Experimental (μStrain)	FEA (μStrain)	% deviation
1	Axle	276	267.9	2.935
2	Stub-axle	18	17.62	2.11
3	Yoke bottom	216	215	0.46
4	Top support	92	92.5	0.543
5	Cylinder	16	16.5	3.0
6	Toggle link	116	117	0.854

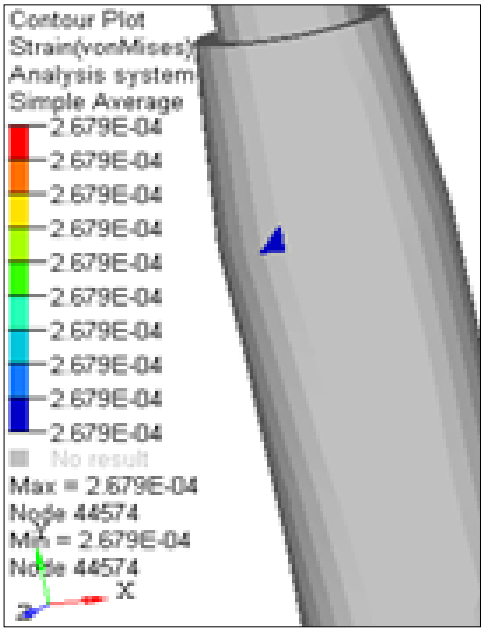

Fig. 16: *Strain Plot on Axle.*

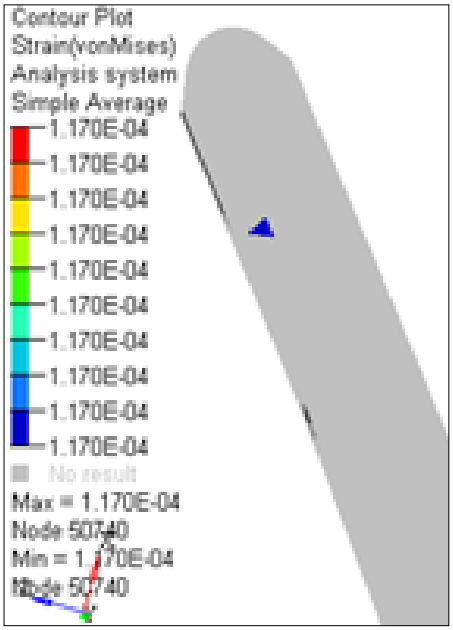

Fig. 17: *Strain Plot Toggle Link.*

Fatigue Analysis

Landing gear are usually subjected to complicated loading conditions during taxiing, take-off and landing of an aircraft, both dynamic and static loads such as gear spin-up and spring back, turning, lateral drift, braking, maximum vertical, taxiing, towing and pushback. To ensure structural integrity of the component, fatigue design load spectra are generated statistically to accumulate the experience of maturing fleets during take-off and landing, various missions and ground handling conditions. The aim is to ensure for designing a landing gear structure against the fatigue limit, that the structural integrity is satisfactory throughout its planned service life. From the landing gear strength calculations, we obtained the stress spectrum which is necessary for Fatigue analysis. Output from Fatigue analysis is either life in cycles or a safety factor depending on the type of analysis was conducted.

Fatigue analysis process is logarithmic. A ten percent error in loading magnitude could result in a 100% error in the predicted fatigue life.

Stress-Life is commonly used for components like Landing gear as is subjected to lower loads within the elastic limit. Figure 18 is a typical loading sequence of Table 7 is shown. Basic requirement of Stress-Life Approach is an S-N (Wohler curve) which represents Stress amplitude versus Number of cycles to Failure. Materials utilized in Landing gear are Aluminum alloy 2024-T3 (Toggle Link) and MAN_TEN Steel alloy data in the form of S-N curves [12] are shown in Figure 19.

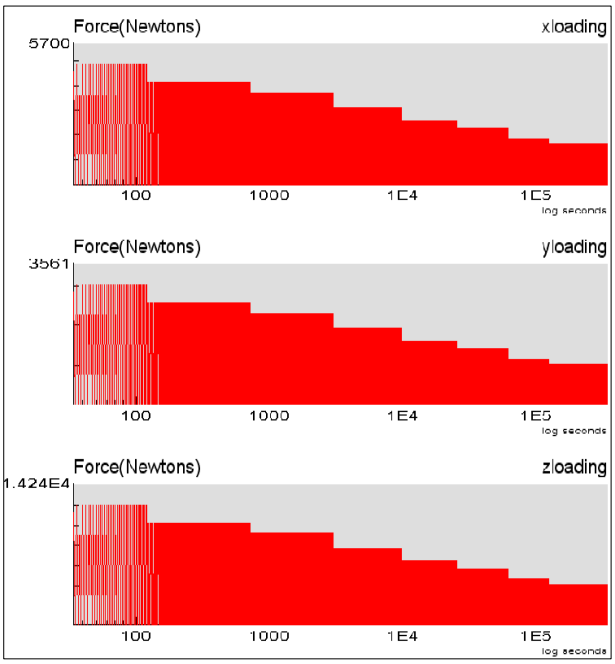

***Fig. 18**: Block Loading Sequence for Table 7.*

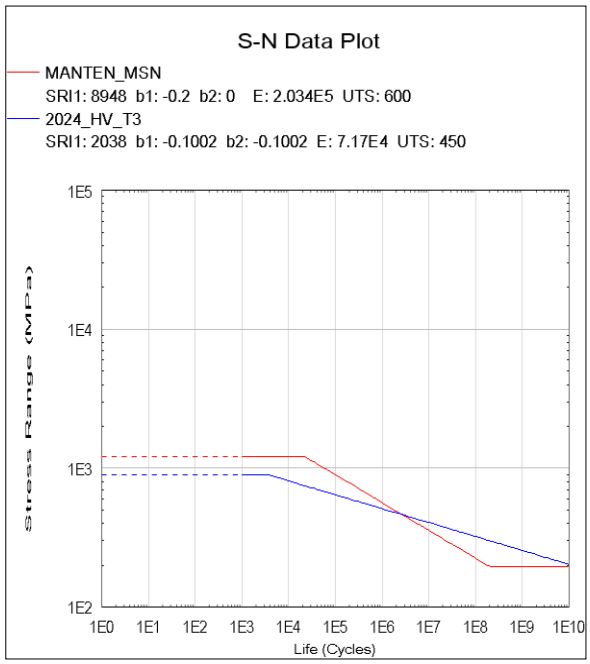

***Fig. 19:** S-N Curve for Two Materials.*

Loading History for Fatigue Analysis

The reactions at the ground during landing at different sinking speeds have been calculated for NLG by the landing gear design group. Table 7 depicts the load verses sinking speed for NLG. Spin-up: As per FAR 25.479 (C) (1) [16] the condition of maximum spin up load, drag components simulating the forces required to accelerate the wheel rolling assembly up to the specified ground speed must be combined with the vertical ground reaction existing at the instant of peak drag load. The coefficient of friction need not exceed 0.8. The spin up is a combination of maximum drag loads and corresponding vertical loads.

Lateral drift landing: The most severe combination of loads that are likely to encounter during a lateral drift landing must be taken into account. In absence of a more rational analysis of this combination, the following must be investigated. The spectrum generated is based on the assumption that this condition is 60% of the total cumulative occurrence of nose gear. The load spectrum for Lateral drift is shown in Table 7 for different sinking speed.

***Table 7:** NLG Load Magnitude in Three Directions for Different Sinking Speed*[17].

Sinking Speed (Ft/sec)	Loads (N)			Cumulative Occurrence per 1 00 000 flights
	Vertical (Z)	Drag (X)	Side (Y)	
1	4 051.53	1 618.65	±1 010.43	1 19 600

2	4 051.53	1 618.65	±1 010.43	96 000
3	4 640.13	1 854.09	±1 157.58	63 600
4	5 699.61	2 285.73	±1 422.45	36 000
5	6 474.6	2 589.84	±1 618.65	15 600
6	7 730.28	3 090.15	±1 932.57	6 800
7	9 201.78	3 678.75	±2 295.54	2 300
8	10 300.5	4 120.2	±2 580.03	600
9	12 144.78	4 855.95	±3 031.29	110
10	14 244.12	5 699.61	±3 561.03	12

The sum of loading sequence in each of the three directions the number of points is 3 40 622 points. The three directions maximum values in X, Y and Z are 5 700, 3 561, and 14 244 respectively. The loading sequence is in the time (seconds) domain. [17, 18]

Since, the Maximum stress occurs at the toggle part of NLG, the fatigue analysis is carried out for only on the toggle link using MS Fatigue Package by creating a group set for the toggle link separately and assigning the material and load spectrum to the components and further the analysis is carried out. A unique loading sequence obtained from actual service load. [19] This spectrum is used for a plate with a hole.

SOLUTION PARAMETERS FOR FATIGUE ANALYSIS

Solution parameters defined forms the core of Fatigue analysis. Stress based models are Maximum Principal as in Eq. (1), Tresca Eq. (2), von-Mises Eq. (3), Mean stress correction (Goodman and Gerber), and setting up for Bi-axial and Factor of Safety analysis. Equation 2 signifies Maximum Shear stress criterion or Tresca criterion. Equation 3 signifies Maximum distortion energy Criterion or von-Mises Stress.

The Equivalent Stress based models used in this document are:
Maximum Principal Stress (Rankine):

$$S_{eq}=\sigma_{1,2}=\frac{\sigma_x+\sigma_y}{2}\pm\sqrt{\left(\frac{\sigma_x-\sigma_y}{2}\right)+\tau_{xy}^2} \quad \text{Eq. (1)}$$

Maximum Shear Stress (Tresca) Criterion:

$$S_{eq}=\frac{1}{2}(\sigma_1-\sigma_2) \quad \text{Eq. (2)}$$

Distortional energy theory (von-Mises):

$$S_{eq}=\frac{1}{\sqrt{2}}\sqrt{(\sigma_x-\sigma_y)^2+(\sigma_y-\sigma_z)^2+(\sigma_z-\sigma_x)^2+6(\tau_{xy}^2+\tau_{yz}^2+\tau_{xz}^2)} \quad \text{Eq. (3)}$$

Mean Stress Correction Models

From the perspective of applied cyclic stresses, the fatigue damage of a component strongly correlates with the applied stress amplitude or applied stress range, and is secondarily influenced by the mean stress. Since, it is not the case of a fully reversed loading case the mean stress effect seriously considered in fatigue analysis. Various theories [20, 21] used for the consideration of mean stress effects are briefly discussed in this document. Goodman relation Eq. (4) is commonly used due to the mathematical simplicity and slightly conservative results. The Gerber relation is quadratic as gave in Eq. (5).

Goodman: $$\frac{\sigma_a}{\sigma_E}+\frac{\sigma_m}{\sigma_u}=1$$ Eq. (4)

Gerber: $$\frac{\sigma_a}{\sigma_E}+\left(\frac{\sigma_m}{\sigma_u}\right)^2=1$$ Eq. (5)

Factor of Safety Analysis

Apart from representing Total Life in fatigue equivalent units, Safety factor is another term commonly used in design life of a component which can also be calculated using the Factor of Safety (FoS) analysis [22] in Stress-Life method.

The FoS analysis is either Stress based or Life based. In general, the Stress-Based method compares the largest stress cycle that occurs in the loading sequence to a reference stress (normally the fatigue limit) taking into account the mean stress.

In order to assess the fatigue life of "infinite life" structures, it has been found most useful if a measure obtained of the difference between the working stress and the fatigue limit stress (an endurance stress below in which no fatigue damage occurs). Often is this expressed as a ratio of fatigue limit/working stress and this ratio is known as the "Factor of Safety" (FoS). The FoS is as shown in Eq. (6).

FoS (Safety Factor) = Working stress/ Endurance stress Eq. (6)

Considering the basic factor of safety concept as a ratio of the applied stress on the fatigue stress, it is possible to introduce a mean stress correction based on Goodman and Gerber rules as showed in Eq. (7) and (8) respectively.

FoS (Safety Factor) based on Goodman = $$\frac{\sigma}{\sigma_a\left[1-\frac{\sigma_m}{\sigma_u}\right]}$$ Eq. (7)

FoS (Safety Factor) based on Gerber = $$\frac{\sigma}{\sigma_a\left[1-\left(\frac{\sigma_m}{\sigma_u}\right)^2\right]}$$ Eq. (8)

FATIGUE ANALYSIS OF A PLATE WITH A HOLE

Consider a square plate 100 × 100 mm with a hole of radius 5 mm at the centre. FE model consists of nodes 11 288 and elements 11 020. Element type used is CQUAD4 four noded isoparametric plate element capable of modelling plane stress and plane strain problems. Shell thickness is given as 1 mm and material used for this is MAN_TEN steel. Both stress and fatigue analysis are carried out in full, half and quarter plate configurations.

The Boundary Condition (BC) for full plate one edge is fixed in all six directions, for half plate the fixed edge is retained as it is and the symmetry edge is restrained with U_y, θ_x, θ_z (2,4,6) = 0 and the quarter plate retain the horizontal edge of half plate, in the vertical edge U_x, θ_y, θ_z (1,5,6) = 0 as shown in Figure 20. The load applied for the full plate is 13 130 N and for half and quarter plates it is 6 565 N.

The stress results for different configurations of a plate are shown in Figures 21, 22 and 23. The displacement and stress results are tabulated in Table 8. Results are compared for different configurations of a plate and damage plot for fully reversed cyclic load is carried out and results as showed in Figures 24, 25 and 26. Table 9 and 10 shows the three models depict life of a plate with a hole and Safety Factor using equivalent stress model.

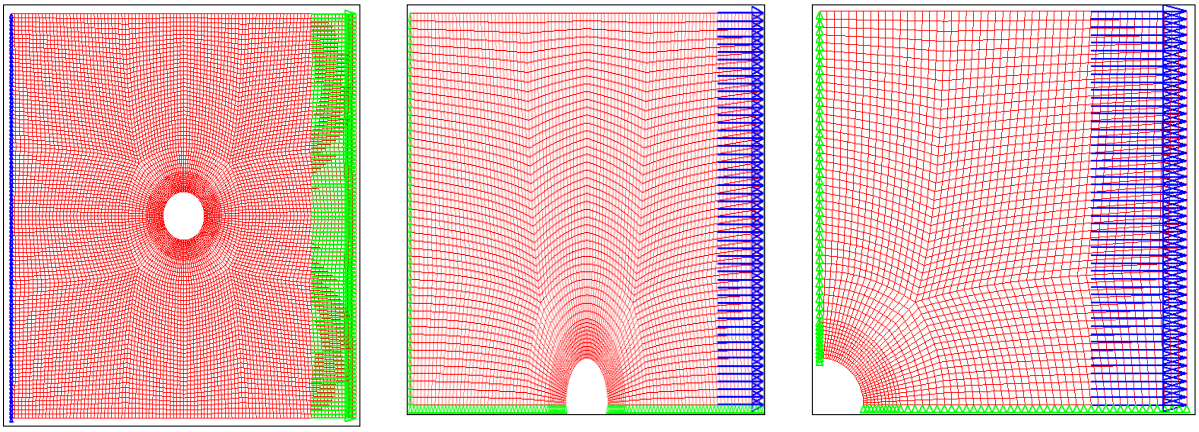

(a) Full plate FE model *(b) Half plate FE model* *(c) Quater plate FE model*

Fig. 20: *Different Configurations of a Plate with Hole.*

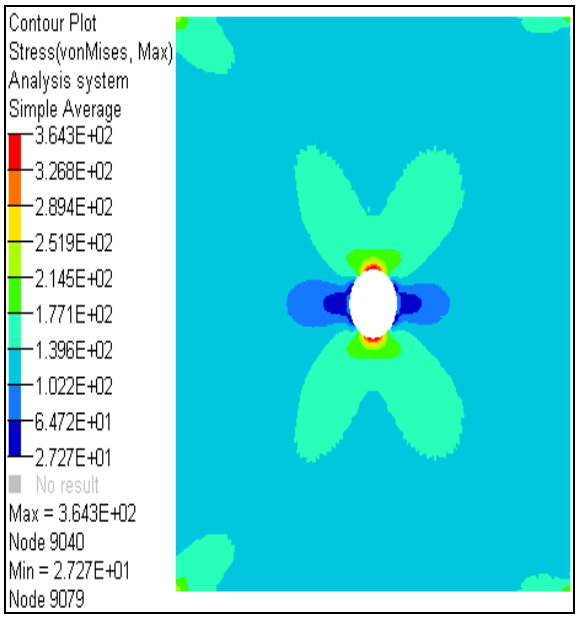

Fig. 21: *Stress Plot on a Full-Plate with Hole.*

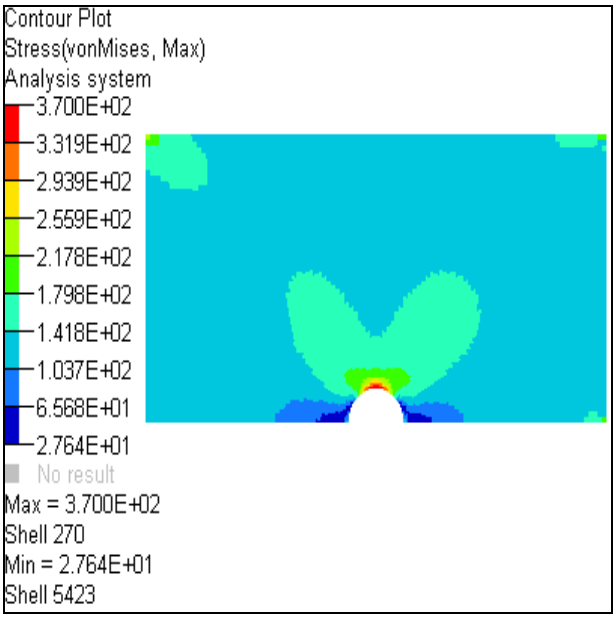

Fig. 22: *Stress Plot on a Half Plate with Hole.*

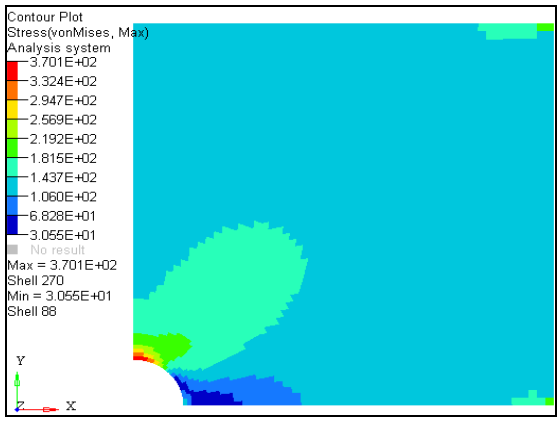

Fig. 23: *Stress Variation on a Quarter Plate.*

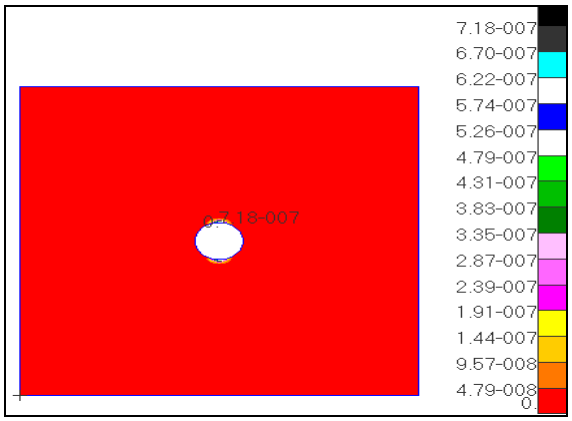

Fig. 24: *Damage Plot- Full Plate With Hole- Goodman Mean Stress - Von Mises.*

Table 8: *Comparison of Full, Half and Quarter Plate δ and σ.*

Description	Nodes	Elements	Displacement (δ, mm)	Stress (σ, MPa)
Full Plate	11288	11020	6.66E-02	364.3
Half Plate	5694	5510	6.731E-02	370
Quarter Plate	2872	2755	3.557E-02	370.1

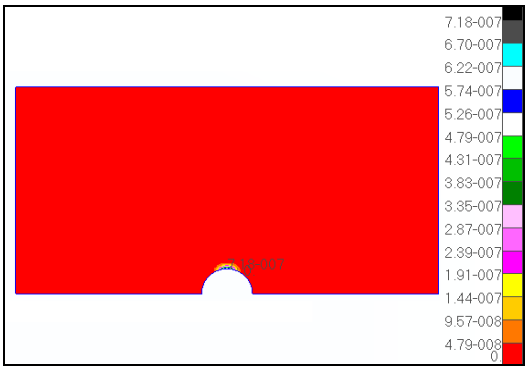

Fig. 25: *Damage Plot -Half Plate with a hole - Goodman Mean Stress - Von Mises*

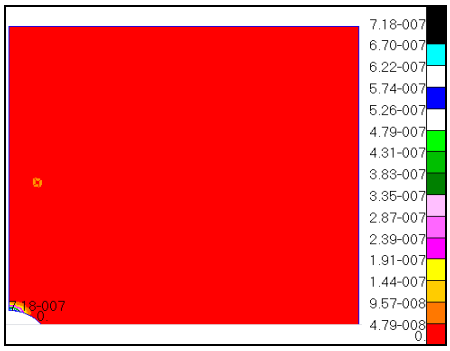

Fig. 26: *Damage Plot- Quarter Plate with a hole- Goodman Mean Stress-Von Mises.*

Table 9: *Three Models Depict Life of a Plate with Hole.*

Life (cycles) Half and Quarter Plate Mean stress	Max Abs-principal	Von-Mises	Critical Plane
None	2.23E05	8.41E06	2.23E05
Goodman	2.00E05	1.39E06	2.00E05

Table 10: *Comparison - Factor of Safety-Equivalent Stress Models.*

Factor of Safety-No mean stress correction		
Max abs Principal	**Von-Mises**	**Critical Plane**
1.11	1.65	1.11

Figure 27 shown the loading sequences[19] which are applied to the quarter plate as a loading history. The cycle histogram distribution of two different sequences of loading is shown in Figure 28. Table 11 shows the rain flow cycles and life in cycles for no mean (none) and Goodman with mean stress correction for a plate subjected to different loading spectrum.

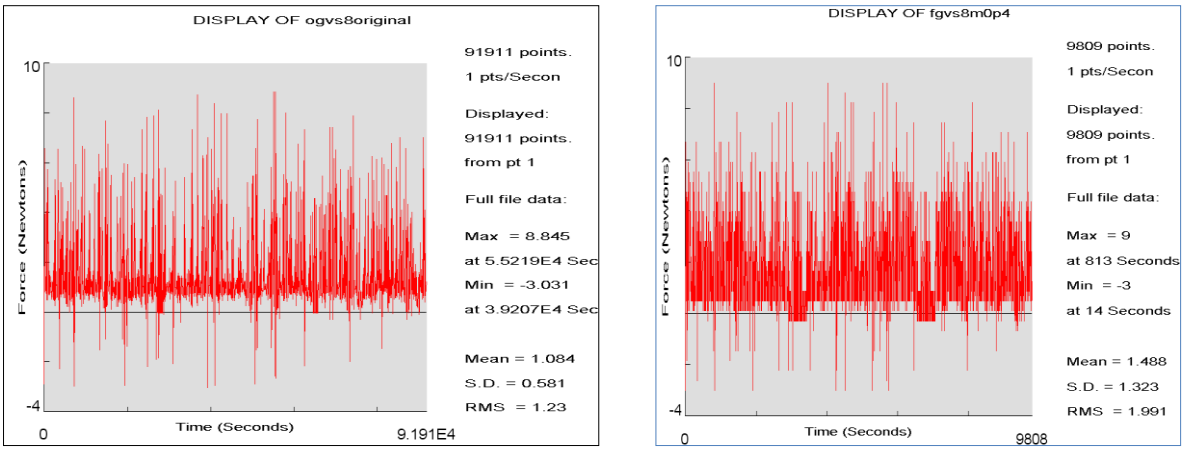

(a) Original loading sequence *(b) Filtered loading sequence*

Fig. 27: *Different Load Cases for a Quarter Plate with a Hole.*

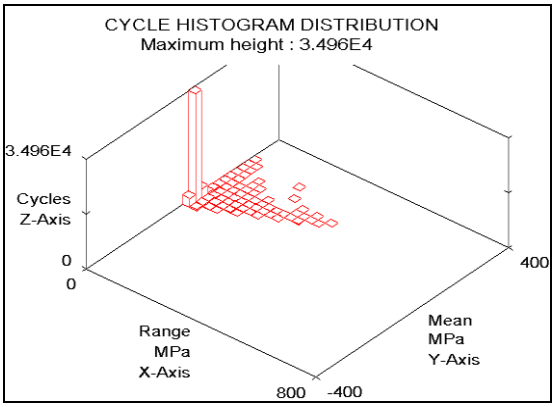

(a) Cycle histogram for original load case

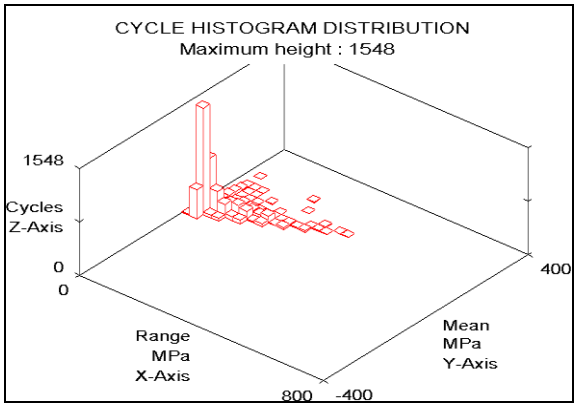

(b) Histogram for zero point four load case

***Fig. 28**: Cycle Histogram for The Loading Sequence for Quarter Plate.*

***Table 11:** Life in Cycles for Four Loading Cases for a Quarter Plate with Hole.*

Description	Load case 1	Load case 2	Load case 3	Load case 4
Number of data points	91 911	21 470	14 675	9 809
Rain flow Cycles	34 960	4 095	2 773	1 548
No Mean Stress (cycles)	3.83E5	2.93E5	2.93E5	2.93E5
Goodman (cycles)	7.30E04	5.5E04	5.5E04	5.5E04

By specifying 99.9% as the design criterion, we calculate a life value based on a 99.9% certainty of survival. The larger scatter of the original S-N data that makes up the curve, the less certain we will be about survival and the code takes this into account by a more conservative manner. The default is a 50% probability of survival (or failure). Table 12 and 13 shows the mean stress correction for 50% and 99.9% certainty of survival respectively.

***Table 12:** Mean Stress Correction Results of Quarter Plate with 50% Survival.*

Mean stress correction (50% Certainty of survival)- load case 2			
MANTEN_MSN	**None**	**Goodman**	**Gerber**
Max prinicpal (cycles)	2.93E05	5.5E04	2.01E05
Scale Factor	1.376	1.415	1.181

***Table 13:** Mean Stress Correction Results of the Quarter Plate with 99.9% Survival.*

Mean stress correction (99.9% Certainty of survival)-load case 2			
MANTEN_MSN	**None**	**Goodman**	**Gerber**
Max prinicpal (cycles)	9.25E04	2.12E04	6.66E04
Scale Factor	1.142	0.8723	1.044

Load case 1 is the original loading sequence has the maximum number of data points as 91 911. This data is subjected to removal of small amplitude of cycles say 0.1, 0.2 (load case 2), 0.3 (load case 3), 0.4 (load case 4) and 0.5 the corresponding data points are 47 254, 21 470, 14 675, 9 809 and 7 661 respectively. These six data points are subjected to rainflow cycle count algorithm in MSC fatigue module the corresponding number of cycles are 34 960, 8 515, 4 095, 2 773, 1 548 and 914. In MSC faigue the stress tensor equation is

$$\sigma_{ij}(t) = P(t)\frac{A\sigma_{ij}}{B} + C. \qquad \text{Eq. (9)}$$

Where A – Scale factor (1), B – Load magnitude (1), C – Offset (0), P(t) – Cyclic load as a variation of time, σ_{ij} – Stress tensor

Default values for the Eq. (9) Constant values are given in small brackets along with the description of the variables. It is important here to note the load magnitude for quarter, half and full plate is taken according to the load spectrum i.e., maximum load spectrum value is 9.

MULTIAXIAL FATIGUE ANALYSIS of NLG

Multiaxial fatigue analysis shows a minimum life predicted by both Von-Mises and Maximum Principal - life of 6.84E07 and 1.63E08 Cycles, for a Toggle Link component considering a Scatter factor of 3. The damage of 6.13E-09 for maximum principal of lateral drift loading shown in Figure 29 corresponds to a life cycle of 1.63E08 and Figure 30 shows the Safety Factor for Toggle link. This corresponds to a total of 7 552 flying hours with a scatter factor of 3. Table 14, 15 and 16 shows the Mean stress correction for 50% certainty of survival, comparison of Equivalent stress models and comparison of Factor of safety-Equivalent stress models respectively.

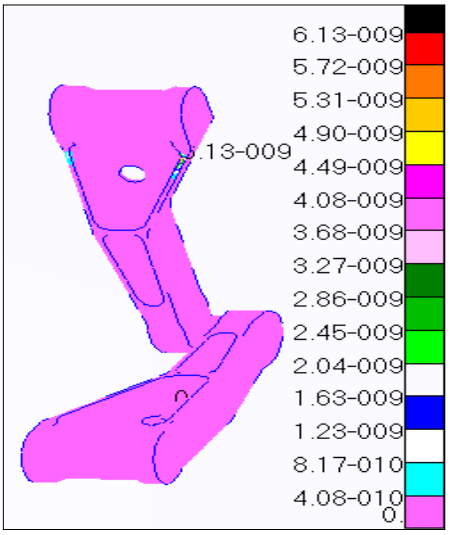

Fig. 29: *Damage Plot -No Mean Stress.*

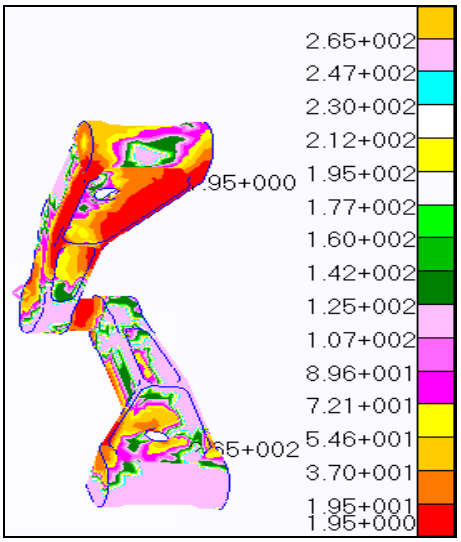

Fig. 30: *Factor of Safety.*

Table 14: *Mean Stress Correction.*

Mean stress correction (50% Certainty of survival)			
Al-2024-T3	**None**	**Goodman**	**Gerber**
Max prinicpal (cycles)	1.63E08	2.2E07	1.18E08

Table 15: *Comparison-Life in Cycles -Equivalent Stress Models.*

Description	**Life (cycles) -Lateral drift landing**		
Mean Stress	**Max Principal**	**Von Mises**	**Critical Plane**
None	1.63E08	6.84E07	9.46E09
Goodman	2.20E07	9.65E06	2.96E09

Table 16: *Comparison –Factor of Safety-Equivalent Stress Models.*

Description	**Factory of safety**		
Mean Stress	**Max Principal**	**Von Mises**	**Critical Plane**
None	1.95	1.84	3.01
Goodman	1.46	1.38	2.55

CONCLUDING REMARKS

1. Modeling of Nose Landing gear is done using 1D beam and 3D tetrahedral elements. The h-type convergence study is done with 1D beam elements with size 2.5, 5 and 10 mm. The results are for 10 mm the maximum stress 185.7 MPa and for 5 mm it is 192.2 MPa and for 2.5 mm it is 192.7 MPa.
2. From Nose Landing gear strength calculations, the maximum stress observed is 220 MPa for Lateral Drift loading case and it occurs in the Upper toggle link component made up of Aluminium alloy with UTS = 490 MPa. Hence, it is cleared from strength point of view.
3. Comparison of Stress results of both Solid and Line model with MPC beam showed variations within 10% accuracy of stress results.
4. One MPC be placed at the lowest point of contact and a myriad of MPCs placed above it yield the same result.
5. Validation of results is done for the Nose Landing Gear (NLG) strength calculation is by comparing with the experimental strain gage tests results and results found to be within 3% variation. This confirms the modeling strategy is good.
6. Fatigue analysis of a plate with hole was carried out with fully reversed loading. This problem has been modeled as full, half and quarter plate. The static stress and fatigue damage remains constant. Later this problem is subjected to unique loading (on-line data acquired from the flight). This loading sequence has been optimized by filtering the lower magnitudes of loading cycles.
7. Higher the percentage of certainty of survival (50–99.9%) lower is the life of component (2.93E05–9.25E04 cycles).
8. The NLG having a life cycle of 1.63E08 corresponds to a total of 7 552 flying hours with a scatter factor of 3.

ACKNOWLEDGMENT

We thank Sri. Shyam Chetty, Director, Dr. J. S. Mathur, Head, KTMD, Dr. Satish Chandra, Head, STTD (Structural Technologies Division), and Dr. VanamUpendranath, IVHM, CSIR-National Aerospace Laboratories, Bangalore, for providing an opportunity and the necessary facilities to carry out this work. We thank the ADA-NPMASS for sponsoring the Landing Gear Health Management project. We thank everyone, directly or indirectly helped us in bringing out this work in the present form.

REFERENCES

1. Currey N.S. *Aircraft Landing Gear Design*: Principal and Practices, American Institute of Aeronautics & Astronautics (AIAA) Inc. 1988, ISBN-0930403-41-X.
2. Praveen Joel P., Vijayan R. Design and Stress Analysis of Nose Landing Gear Barrel (NLGB) of a typical naval trainer aircraft. *IOSR Journal of Mechanical and Civil Engineering.* 2014; 11.
3. http://www.ecfr.gov/cgi-bin/text-idx?tpl=/ecfrbrowse/Title14/14cfr23_main_02.tpl (09Dec. 2014)
4. Nguyen T.D. *Finite Element Analysis of a Nose Gear during Landing*. University of North Florida, Master of Science thesis in Mechanical Engineering, 2010.
5. Darrell F. Socie, Gary B. Marquis. *Multiaxial Fatigue*. SAE International, Commonwealth Drive, Warrendale, PA 15096-0001. ISBN:0-7680-453-5, (2000).
6. Liu Y., Mahadevan S. Multiaxial high-cycle fatigue criterion and life prediction for metals. *International*

Journal of Fatigue. 2005; 27: 790–800p.
7. Lok S.K., Paul J.M., Upendranath V. Prescience Life of Landing Gear using Multiaxial Fatigue Numerical Analysis. *Procedia Engineering*. 2014, 86: 775–9p.
8. Carpinteri A., Spagnoli A. Multiaxial high-cycle fatigue criterion for hard metals. *International Journal of Fatigue.* 2001; 23: 135–45p.
9. Papuga J. A survey on evaluating the fatigue limit under multiaxial loading. *International Journal of Fatigue.* 2011; 33: 153–6p.
10. Bong-Ryul You, Soon-bok Lee. A critical review on Multiaxial fatigue assessments of metals. *International Journal of Fatigue.* 1996; 18(4): 235–44p.
11. Abaqus CAE User's manual 6.10 Dassault systems/simulia, France 2010
12. Military handbook. *Metallic materials and Elements for aerospace vehicle structures*. MILHDBK5G-VOL1&11: Material Data. 1986.
13. Altair Engineering. 2012, *Hyper Mesh user's manual ver. 9, USA*.
14. Gokhale N.S., Deshpande S.S., Bedekar S.V., *et al*. *Practical Finite Element Analysis*. ISBN:978-81-906195-0-9, January 2008.
15. PATRAN (MSC Fatigue) and NASTRAN 2013. *Software Package, Finite Element Analysis.* California; US: 2007.
16. FAR part 25, *Airworthiness Standards Transport Category Airplanes*. May 2009 Edn.
17. A. Rinku, Naveena M. Report on Fatigue spectrum for medium scale transport aircraft's Landing Gear. XXXXX/STR/50, 2007.
18. Singh K.L., Chakrabarti P., Chandra S. *Report on Computation of NLG and MLG Landing Loads*. NCAD/DQ-04/0005/2012, 21March 2012.
19. Singh K.L., Venkata Subramanyam D.V. Techniques to Generate and Optimize the Load Spectra for an Aircraft. *International Journal of Mechanics and Materials in Design*. March 2010, DOI: 10.1007/s10999-010-9121-7.
20. Bishop N.W.M., Sherratt F. Finite Element Based Fatigue Calculations.NAFEMS. *The International Association for the Engineering Analysis Community*. 2000.
21. Lorand K. Review of high cycle fatigue models applied for multi axial tension-torsion loading based on new accuracy assessment parameter. *Journal of Engineering Studies and Research*. 2012; 18(3): 75–86p.
22. Lee Y.L., Markey M.E., Kang H.T. *Metal Fatigue analysis Handbook. Butterworth-Heinemann*. Elsevier; ISBN 978-0-12-385204-5. 2012.
23.